UNIVERSITÀ
DEGLI STUDI DI BARI
ALDO MORO

DIPARTIMENTO INTERATENEO DI FISICA "M. MERLIN"

**Tesi di laurea Magistrale in**
**"Nuclear, Subnuclear and Astroparticle Physics"**

# Search for $\tau \to 3\mu$ decays using $\tau$ leptons produced in D and B mesons decays in CMS experiment at LHC

Relatrici:
**Dott.ssa Anna Colaleo**
**Dott.ssa Rosamaria Venditti**

Laureanda:
**Caterina Aruta**

**Anno Accademico 2018-2019**

# Contents

# Chapter 1

# Standard Model and new physics searches

The *Standard Model* (SM) of particle physics is the theory that we use to describe the fundamental blocks of the matter and the forces that govern their interaction. This theory includes three of the four known fundamental forces (electromagnetic, weak and strong interactions), leaving aside the gravitational force, which is also the weakest one. This is the reason why this model provides extremely precise predictions even if it is not complete.
The SM was finalized only in mid-1970s and it has predicted a variety of physics phenomena and successfully explained almost all the experimental results obtained up to now.
However, it is evident that it is an effective theory, and therefore it needs to be extended in order to include the gravitation and to provide a description of some experimental observations which are still unexplained.
For these reasons, in the last years some extensions of the SM have been developed and their predictions are continously under test in order to be rejected or confirmed.

## 1.1 The Standard Model

### 1.1.1 Fundamental particles and gauge symmetries

The Standard Model classifies the particles according to their intrinsic angular momentum, the spin, dividing them in two main categories, as shown in Fig. 1.1.

- **Bosons**: particles with integer values of the spin. They follow Bose-Einstein statistics and are defined as the carriers of the fundamental interactions. The photon $\gamma$ is the carrier of the electromagnetic force, the weak force is mediated by $W^{\pm}$ and Z bosons and the strong force is mediated by gluons. In the SM there is also another boson, called *Higgs* boson, which is not a force mediator but it is a scalar boson arising from a spontaneous symmetry breaking phenomenon, the mechanism responsible for particles masses.

- **Fermions**: particles with semi-integer values of the spin. They obey Fermi-Dirac statistics and some of them are the elementary blocks that constitute the observable matter. Fermions are divided in 2 groups: *leptons* (which have an integer electric charge) and *quarks* (characterized by a fractional electric charge).
  Each of these group is made up of 6 particles, paired in 3 generations (or families), as shown in the Fig. 1.1. Each of the three charged leptons (electron, muon and tau) has a corresponding neutrino, which has no electric charge. Each quark pair, instead, is made up of two quarks with electric charges respectively equal to $\frac{2}{3}$ and $-\frac{1}{3}$.
  For each of this 12 different fermions there is a corresponding antiparticle, characterized by the same mass and spin, but opposite value for the other quantum numbers. Therefore, in total, the model distinguishes 24 fermions.

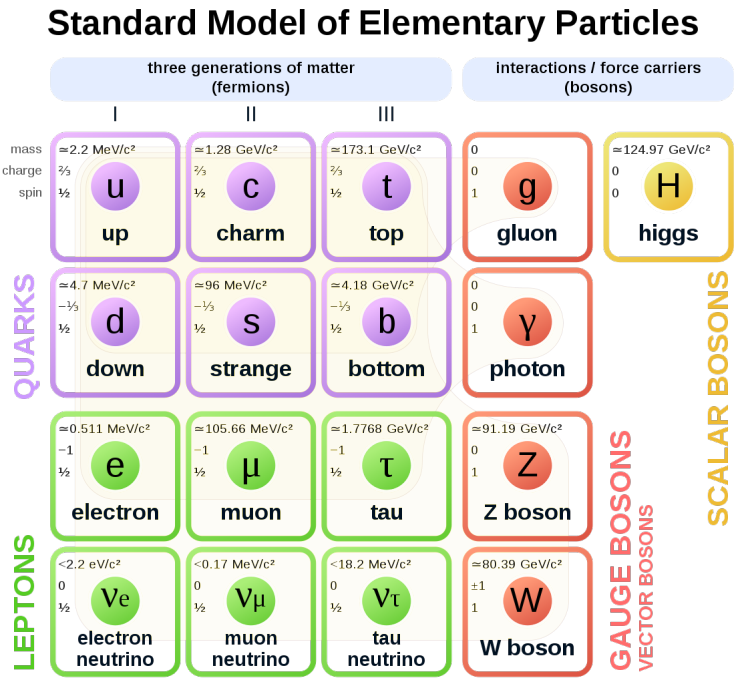


**Figure 1.1:** A summary table with all the SM particles: the fermions (on the left), which are the matter particles, are divided into quarks (in violet) and leptons (in green), while the bosons (on the right), are classified into gauge bosons, i.e. the carriers of the interactions (in red) and the scalar Higgs boson (in yellow). For each particle, the mass, electric charge and spin values are reported.

The fundamental symmetry group that is gauged in the Standard Model is

$\mathrm{SU(3)_C} \otimes \mathrm{SU(2)_L} \otimes \mathrm{U(1)_Y}$ , where:

- $\mathrm{SU(3)}_C$ is the symmetry group at the basis of the Quantum Cromodynamics (QCD), the theory that describes the interaction between quarks and gluons,
- $\mathrm{SU(2)}_L \otimes \mathrm{U(1)}_Y$ is the gauge group for the electroweak interactions. $\mathrm{U(1)}_Y$ is different from $\mathrm{U(1)}_{em}$, the symmetry group at the basis of the Quantum Electro Dynamics

(QED), the theory that describes the electromagnetic interactions. In fact, the generator of $U(1)_{em}$ is the electromagnetic charge Q, while the hypercharge $Y$ is the generator of $U(1)_Y$ .

**Quantum Chromodynamics (QCD)**

The Quantum Chromodynamics [1] describes the interaction between quarks and gluons. Each quark can be characterized by three different values of a quantum number, called *color*. However, in nature only colorless states can be observed, and this is explained by the fact that these states are singlets under rotations in color space $SU(3)_C$. A consequence of this so-called *confinement hypothesis* is that quarks can never be observed as free particles (because they carry color) and they are always confined within color-singlet bound states.

The symmetry group $SU(3)_C$ is non-Abelian, and this is the reason why the QCD phenomenology is completely different from that of QED, which is describes by the $U(1)_{em}$ group, that is Abelian. One of the most relevant consequences of this, is the fact that gluons are self-interactive.

The generators of $SU(3)_C$ are the matrices $T^a = \frac{\lambda^a}{3}$, where $a$ = 1,...,8 (the dimension of the group) and the $\lambda^a$ are the *Gell-Mann matrices*. The group algebra is defined by: $[T^a,\ T^b] = if^{abc}T^c$.
Since quarks are fermions, the Lagrangian density of free quarks can be written as in 1.1.

$$\mathcal{L}_q(x) = \sum_{j=1}^{f} \bar{q}^j(x)\ (i\gamma^\mu\partial_\mu - m_j)\ q^j(x) \tag{1.1}$$

where, for every possible flavor labelled by $j$, each matter field is given by $q^j$ that takes into account the three color states: $q^j = \begin{pmatrix} q_1^j \\ q_2^j \\ q_3^j \end{pmatrix}$

The Lagrangian in 1.1 is invariant under global transformations belonging to $SU(3)_C$, i.e. transformations not depending on the particular spacetime point in which they are performed, but it is not invariant under local ones (called *gauge* transformations), which can be written as: $q(x) \to q'(x) = U(x)q(x)$.
The gauge invariance of physics theories is a crucial requirement, that has to be fulfilled in order to, in other words, make the physics description universal and not depending on particular cases.

The gauge invariance can be restored by introducing 8 vector fields, the gluons, defined as: $G_\mu(x) = G^a_\mu(x)\frac{\lambda_a}{2}$, which are hermitian and traceless. Moreover, the minimal coupling between the quarks and the gluons can be introduced by replacing the derivative with a covariant derivative $D_\mu$, defined as: $D_\mu = \partial_\mu + ig_sG_\mu(x)$, being $g_s$ the dimensionless coupling constant of the strong forces.
Finally, the Lagrangian density in 1.1 is invariant under gauge transformations iff the gluon fields transform as: $G_\mu(x) \to G'_\mu(x) = U(x)G_\mu(x)U^\dagger(x) - \frac{i}{g_s}U(x)\partial_\mu U^\dagger(x)$.

A last addition to the Lagrangian has to be made, in order to include the gluon dynamics, which is still missing. In order to do it, a *gluon field strength tensor* $G_{\mu\nu}$ must be introduced. It is defined as: $G_{\mu\nu}(x) = \partial_\mu G_\nu(x) - \partial_\nu G_\mu(x) + ig_s[G_\mu(x), G_\nu(x)]$ and its components are: $G_{\mu\nu}(x) = G^a_{\mu\nu}(x)\frac{\lambda_a}{2}$.

The gauge invariant QCD Lagrangian density is given by the equation 1.2.

$$\mathcal{L}_{QCD} = -\frac{1}{4}\, G^a_{\mu\nu}(x)G^{\mu\nu a}(x) + \sum_{j=1}^{f} \bar{q}^j(x)\ (i\gamma^\mu D_\mu - m_j)\ q_j(x) \tag{1.2}$$

$SU(3)_C$ is an exact symmetry: in 1.2 there is not a term $\propto G^\mu G_\mu$ because it would be $\propto m^2$ and it would break the invariance. Therefore gluons, like photons in QED (where also $U(1)_{em}$ is an exact symmetry), are massless, and they have a spin value equal to 1.
Moreover, expanding the term $G_{\mu\nu}G^{\mu\nu}$ present in the Lagrangian, it is possible to find explicitly the contributions which describe the self-interaction of three or four gluons.

**Electroweak theory**

The electroweak theory is the product of the unification of the QED and the weak theory, carried out by Glashow in 1961 [2]. It is described by the gauge group $SU(2)_L \otimes U(1)_Y$, where $SU(2)_L$ is the *left-handed weak isospin group* and $U(1)_Y$ is the *hypercharge* group. The hypercharge $Y$ and the electromagnetic charge $Q$ are related by the equation $Q = \frac{Y}{2} + T_3$, where $T_3$ is the third component of the weak isospin.
The generators of $SU(2)_L$ are the three matrices $T^a = \frac{\sigma^a}{2}$, where a=1,2,3 and $\sigma^a$ are the *Pauli* matrices. They satisfy the algebra: $[T^a,\ T^b] = i\epsilon^{abc}T^c$.
The generator of $U(1)_Y$ is the matrix $Y$ defined as: $Y = \begin{pmatrix} y_L & 0 & 0 \\ 0 & y_L & 0 \\ 0 & 0 & y_R \end{pmatrix}$.
$SU(2)_L \otimes U(1)_Y$ is not a *simple* group, therefore it is characterized by two coupling constants: $g$ for $SU(2)_L$ and $g'$ for $U(1)_Y$.

The matter fields of this theory are leptons and quarks. Experimental observations have shown that, while charged leptons can be both left-handed and right-handed, neutrinos are always left-handed.
For this reason, a family of leptons ($l$) can be arranged in a left-handed part $\begin{pmatrix} \nu_l \\ l_L \end{pmatrix}_L$, which behaves as a doublet for $SU(2)_L$ transformations, and a right-handed part, constituted only by the right-handed charged lepton, $l_R$, which behaves as a singlet.
On the other hand, these two components transform under the action of a local $U(1)_Y$ symmetry, as:

$$\psi \ \rightarrow \ \begin{pmatrix} e^{iy_L\alpha(x)} & 0 & 0 \\ 0 & e^{iy_L\alpha(x)} & 0 \\ 0 & 0 & e^{iy_R\alpha(x)} \end{pmatrix} \psi,$$

where, from experimental evidences, $y_L = -\ \frac{1}{2}$ and $y_R = -1$.

The same can be done with a quark family, but in this case all the quarks, unlike neutrinos, have a right-handed component. For example, for the first family of quarks, the left-handed component is: $\begin{pmatrix} u \\ d \end{pmatrix}_L$, while the right-handed one can be given by both: $u_R$ and $d_R$.

If we put together all the left-handed matter fields in a multiplet $\psi_L$ and the righ-handed ones in $\psi_R$, the gauge invariant Lagrangian density of the electroweak theory is the one in 1.3.

$$\mathcal{L} = \bar{\psi}_L \; i \; \gamma^\mu D_\mu \psi_L + \bar{\psi}_R \; i \; \gamma^\mu D_\mu \psi_R - \; \frac{1}{4} \; W_{\mu\nu} W^{\mu\nu} - \; \frac{1}{4} \; B_{\mu\nu} B^{\mu\nu} \tag{1.3}$$

where:

- $D_\mu$ is the covariant derivative, defined as: $D_\mu = \partial_\mu + igW_\mu + ig'B_\mu Y$.
  $W_\mu$ and $B_\mu$ are the vector gauge fields introduced in order to guarantee the gauge invariance of the theory. They are hermitian and traceless, and in particular, $W_\mu$ is defined as: $W_\mu = W_\mu^a \; \frac{\sigma^a}{2}$.
  These fields must respect the following transformations rules for local symmetries (respectively belonging to $\mathrm{SU}(2)_L$ for $W_\mu$ and to $\mathrm{U}(1)_Y$ for $B_\mu$):
  $W_\mu(x) \; \rightarrow \; W'_\mu(x) = U(x) W_\mu(x) U^\dagger(x) - \frac{i}{g} U(x) \partial_\mu U^\dagger(x)$ ,
  $B_\mu(x) \; \rightarrow \; B'_\mu(x) = B_\mu(x) - \frac{i}{g'} \partial\alpha(x)$

- $W_{\mu\nu}$ and $B_{\mu\nu}$ are the two field strength tensors, defined respectively as:
  $W_{\mu\nu} = \partial_\mu W_\nu - \partial_\nu W_\mu + ig[W_\mu, \; W_\nu]$ ,
  $B_{\mu\nu} = \partial_\mu B_\nu - \partial_\nu B_\mu$

The covariant derivative contains the interaction terms which describe all the possible couplings. It is possible to define:

- two charged gauge fields, by combining the vector fields $W^1$ and $W^2$:

$$W_\mu^\pm = \frac{W_\mu^1 \mp W_\mu^2}{\sqrt{2}}$$

- two neutral gauge fields, by combining the vector fields $W^3$ and $B$:

$$Z_\mu = \frac{gW_\mu^3 - g'B_\mu}{\sqrt{g^2 + (g')^2}}, \qquad A_\mu = \frac{g'W_\mu^3 + gB_\mu}{\sqrt{g^2 + (g')^2}}$$

These last two fields can be seen as a rotation of an angle $\theta_W$, called *Weinberg angle*, of the original $W^3$ and $B$ fields. Therefore they can be written as:

$$Z_\mu = \cos\theta_W W_\mu^3 - \sin\theta B_\mu, \qquad A_\mu = \sin\theta_W W_\mu^3 + \cos\theta B_\mu$$

where: $\cos\theta_W = \frac{g}{\sqrt{g^2+(g')^2}}$ and $\sin\theta_W = \frac{g'}{\sqrt{g^2+(g')^2}}$.

With these definitions it is possible to distinguish three kinds of electroweak interactions:

- *Charged currents*: interactions mediated by $W^{\pm}$ bosons, characterized by a final state with an electrical charge which is different from the one in the initial state.
- *Neutral currents*: interactions mediated by the $Z$ boson, which couples with neutrinos but not with right-handed charged leptons, characterized by no change of the electrical charge value in the passage from the initial to the final state.
- *Electromagnetic currents*: interactions characterized by the coupling of the $Z$ boson with charged fermions. It can be seen that the QED can be recovered by putting: $e = g\sin\theta_W = g'\cos\theta_W$.

### 1.1.2 Spontaneous Symmetry Breaking

After the unification of the electromagnetic and weak interaction, described in 1.1.1, there was still a not negligible problem in the theory: all the matter particles involved, as well as the gauge bosons that mediate the weak interaction, were massless. In fact, even if these bosons, at the beginning of 1960's, were not yet been discovered [3, 4], they were expected to be quite massive because of the characteristics of the weak interaction.
However, it was not possible to add explicitly mass terms in the electroweak Lagrangian because that would have violated the gauge invariance, leading to a non-renormalizable theory.

In order to overcome this problem, Weinberg and Salam, with the contribution of Veltmann and 't Hooft, integrated in the theory a *Spontaneous Symmetry Breaking* (SSB) mechanism, hypothesized in 1964 independently by Higgs [5, 7] and by Englert and Brout [6]. This mechanism was able to explain the mass of the particles without violating the gauge invariance of the theory. Contributions from Guralnik, Hagen and Kibble [8] were also fundamental to understand its properties.

A SSB occurs in physics when the vacuum state of a system (the lowest energy state) is not invariant under a symmetry transformation of the Lagrangian.
In order to introduce a SSB in the model described so far, let's consider two complex scalar fields $\phi_1$ and $\phi_2$, which form a doublet in $\mathrm{SU}(2)_L$, transforming under a local transformation as:

$$\phi(x) = \begin{pmatrix} \phi_1(x) \\ \phi_2(x) \end{pmatrix} \rightarrow \phi'(x) = U(x)\phi(x)$$

Moreover, this doublet transforms under a local transformation of $\mathrm{U}(1)_Y$ as:
$\phi(x) \rightarrow \phi'(x) = e^{iy_H\alpha(x)}\phi(x)$, where $y_H$ is the so-called *Higgs hypercharge* and it results to be equal to $\frac{1}{2}$.

The Lagrangian density which describes the dynamics of $\phi$ is the one in 1.4.

$$\mathcal{L}_H = (D_\mu\phi)^\dagger(D^\mu\phi) \; - \; V(\phi^\dagger\phi) \tag{1.4}$$

The covariant derivative, used to guarantee, as usual, the gauge invariance of the theory, is defined as: $D_\mu = \partial_\mu + igW_\mu + ig'B_\mu y_H$.

A potential suitable for a spontaneous symmetry breaking is shown in 1.5.

$$V(\phi^\dagger\phi) = k\ (\phi^\dagger\phi) + \lambda\ (\phi^\dagger\phi)^2 = \frac{k}{2}\rho^2 + \frac{\lambda}{4}\rho^4 \tag{1.5}$$

with $k < 0$ and $\lambda > 0$, having posed: $\frac{\rho}{\sqrt{2}} = \sqrt{\phi^\dagger\phi}$ .

Considering the potential as a function of $\rho$, if $\rho$ is not dependent on $x$, it has two stable equilibrium states, at: $\pm\rho_0 = \pm\sqrt{-\frac{k}{\lambda}}$ and one unstable equilibrium state at $\rho = 0$, as shown in Fig. 1.2.

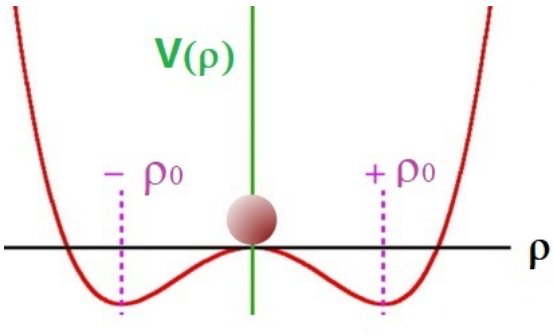


**Figure 1.2:** 1D representation of the Higgs potential as a function depend only on $\rho$.

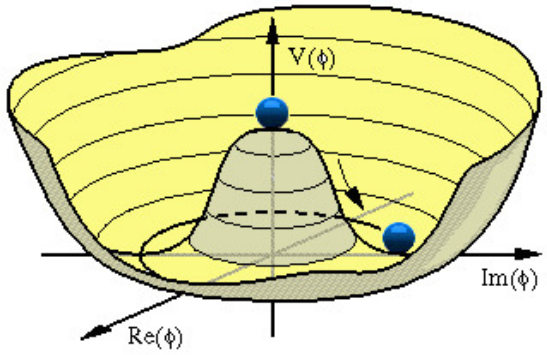


**Figure 1.3:** Higgs potential as a function of the real and imaginary parts of the scalar field $\phi$.

The scalar field can be written as:

$$\phi = e^{i\boldsymbol{\varphi}\cdot\frac{\boldsymbol{\sigma}}{2}} \begin{pmatrix} 0 \\ \frac{\rho_0}{\sqrt{2}} \end{pmatrix} ,$$

where $\boldsymbol{\sigma}$ are the Pauli matrices and $\boldsymbol{\varphi}$ is a constant. In this representation it is possible to notice easier the symmetry of the field, which is shown in Fig. 1.3.
A spontaneous symmetry breaking occurs when the system goes from the initial unstable state, characterized by $\rho = 0$, to one of the infinite degenerate vacuum states, characterized by $\rho = \rho_0$.

The Higgs field $\phi$ has four free parameters (the real and imaginary parts of the two scalar complex fields), therefore it adds four degrees of freedom to the theory. When the field $\phi$ finds its ground state, three of them become the transverse polarization modes of the $W^\pm$ and $Z$ bosons, which therefore become massive (since the Lorentz invariance for massless particles prohibits a transverse polarization of a spin-1 vector particle). The last degree of freedom gives rise to an excitation mode of the field $\phi$ above its ground state: the Higgs boson, a new scalar particle.

- PDG The Higgs field couples to the W$\mu$ and B$\mu$ gauge fields associated with the SU(2)L × U(1)Y local symmetry through the covariant derivative appearing in the kinetic term of the Higgs Lagrangian.

The Higgs boson is neutral under the electromagnetic interactions and transforms as a singlet under SU(3)C and hence does not couple at tree level to the massless photons and gluons.

The fermions of the SM acquire mass through the interactions between the Higgs field and the fermions: the Yukawa interactions, (vedi PDG per la lagrangiana)

**Higgs boson properties**:

- SM Higgs boson is a CP-even scalar of spin 0.
- Higgs mass: $m_H^2 or m_H = 2\lambda\rho_0^2$, where $\lambda$ is the Higgs self-coupling parameter in the potential. It is a free parameter in the SM, and hence, there is no a priori prediction for the Higgs mass.
  The experimentally measured Higgs mass, $m_H \approx$125 GeV, implies that $\lambda \approx 0.13$.
- The vacuum expectation value $\rho_0$ results to be : $\rho_0 = (\sqrt{2}G_F)^{-\frac{1}{2}} \approx$246 GeV, sets the scale of electroweak symmetry breaking. It is fixed by the Fermi constant $G_F$ and it is determined with a precision of 0.6 ppm from muon decay measurements.
- The Higgs boson couplings to the fundamental particles are set by their masses. Mass is thus a dynamic property of elementary particles due to their interaction with the Higgs field, distinct from other intrinsic properties of particles like charge or spin.This is also true for the Higgs boson itself, which owes its mass to its own interaction with the Higgs field.
  The SM Higgs couplings to fundamental fermions are linearly proportional to the fermion masses, whereas the couplings to bosons are proportional to the square of the boson masses.
- etc. pag 183

- From PDG as the SM Higgs boson is a scalar particle, at the quantum level it has sensitivity to high energy thresholds. Quite generally, the Higgs mass is affected by the presence of heavy particles and receives quantum corrections proportional to highest energy scale which destabilize the weak scale barring a large fine tuning of unrelated parameters. This is known as the hierarchy or naturalness problem. There are two broad classes of models addressing the naturalness problem:

1. based on a new fermion-boson symmetry in nature called supersymmetry (SUSY). in this case, the Higgs boson remains elementary and the corrections to its mass are screened at the scale at which SUSY [REF PDG] is broken and remain insensitive to the details of the physics at higher scales. These theories predict at least three neutral Higgs particles and a pair of charged Higgs particles. One of the neutral Higgs bosons, most often the lightest has properties that resemble those of the SM Higgs boson.
2. The other approach invokes the existence of strong interactions at a scale of the order of a TeV or above and induces strong breaking of the electroweak symmetry [REF PDG] In the original incarnation of this second approach, dubbed technicolor, the strong interactions themselves trigger EWSB without the need of a Higgs boson.

In the original incarnation of this second approach, dubbed technicolor, the strong interactions themselves trigger EWSB without the need of a Higgs boson.

– The naturalness problem has been the prime argument for new physics at the TeV scale, and sizable effects on the Higgs boson properties were expected.

### 1.1.3 Finally, the SM

The Standard Model Lagrangian is given in 1.6. It contains, in sequence, the gauge Lagrangian (describing the dynamics of the free fields), the electroweak interaction-not sure-, the Higgs terms and the Yukawa Lagrangian.

$$\mathcal{L}_{SM} = -\frac{1}{4}G_{\mu\nu}G^{\mu\nu} - \frac{1}{2}W_{\mu\nu}W^{\mu\nu} - \frac{1}{4}B_{\mu\nu}B^{\mu\nu} + \bar{\psi}i\gamma^{\lambda}D_{\lambda}\psi + (D_{\lambda}\phi)^{\dagger}(D^{\lambda}\phi) - V(\phi) + \mathcal{L}_{Yukawa} + hermitianconju \tag{1.6}$$

where:

- $\mathcal{L}_{Yukawa}$ is the Yukawa Lagrangian, which describes the coupling between the Higgs field and massless quark and lepton fields. It is given by: $-g\bar{\psi}\phi\psi$
- the covariant derivative $D_\mu$ is defined as: $D_\mu = \partial_\mu + ig_s G^a_\mu F^a + igW^b_\mu T^b + ig'B_\mu Y$
- the matter fields are described by the multiplet: $\psi = \begin{pmatrix} \begin{pmatrix} \nu_l \\ l \end{pmatrix}_L \\ b'_R \end{pmatrix}$.
- the Higgs field $\phi$ is defined as: $\phi = \frac{\rho_0}{2}\begin{pmatrix} 0 \\ 1 + \frac{\rho'}{rho_0} \end{pmatrix}$

### 1.1.4 The discovery of the Higgs boson

The ATLAS and CMS experiments at the Large Hadron Collider, on the 4th of July 2012 announced that they had observed a new particle, (which seemed) consistent with the Higgs boson predicted by the SM, in the mass region around 125 GeV [9, 10].
In the successive years the properties of this particle have been studied i

(In particular, the SM Higgs boson couplings to fundamental fermions are linearly proportional to the fermion masses mf (yf = mf $/\nu$ where yf is the Yukawa coupling) whereas the couplings to bosons are proportional to the squares of the boson masses. As consequence, the dominant mechanism for Higgs boson production and decay involve the coupling of H to W, Z and/or the third generation quarks and leptons. The Higgs boson coupling to gluons is induced at leading order by a one-loop process in which H couples to a virtual $t\bar{t}$ pair. Likewise, the Higgs boson couplings to photon is also generated via loops, although in this case the one-loop graph with a virtual W+W- pair provides the dominant contribution and the one involving a virtual $t\bar{t}$ pair is subdominant.)

### Beautiful plots collection

The distribution of the four-lepton reconstructed invariant mass with full Run 2 data collected at 13 TeV by CMS and ATLAS experiments is shown in Fig. 1.4.

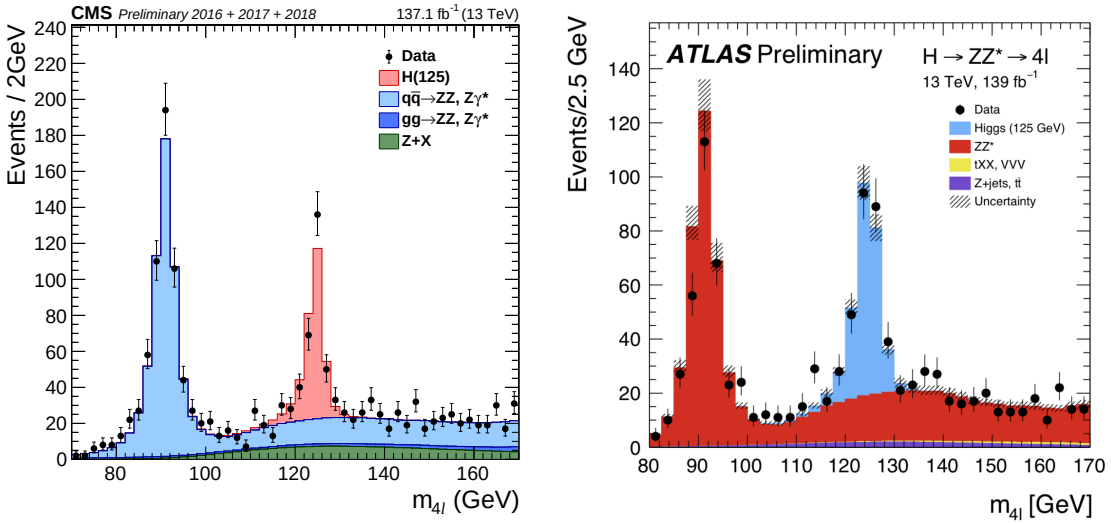


**Figure 1.4:** Distribution of the reconstructed four-lepton invariant mass $m_{4l}$ in the low-mass range, with full Run 2 data, in CMS [11] (on the left) and ATLAS [12] (on the right) experiments. Points with error bars represent the data and stacked histograms represent expected distributions of the signal and background processes.

The distribution of the diphoton reconstructed invariant mass with data collected by CMS and ATLAS experiments at 13 TeV is shown in Fig. 1.5.

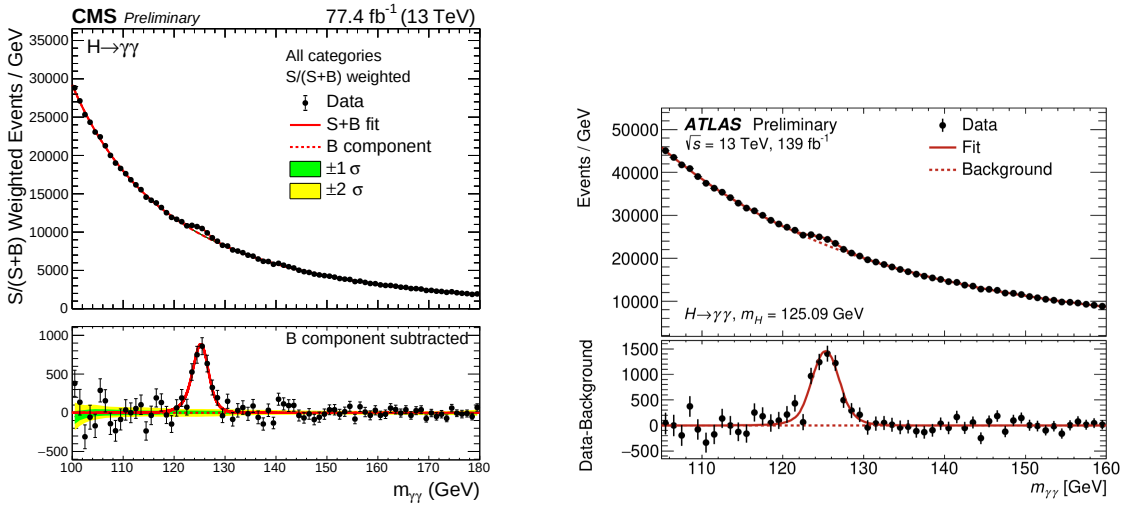


**Figure 1.5:** Distribution of the reconstructed four-lepton invariant mass $m_{2\gamma}$ in the low-mass range, with 2016 and 2017 data collected by CMS [13] (on the left) and the full Run 2 data collected by ATLAS [14] (on the right). The black dots represent the data.

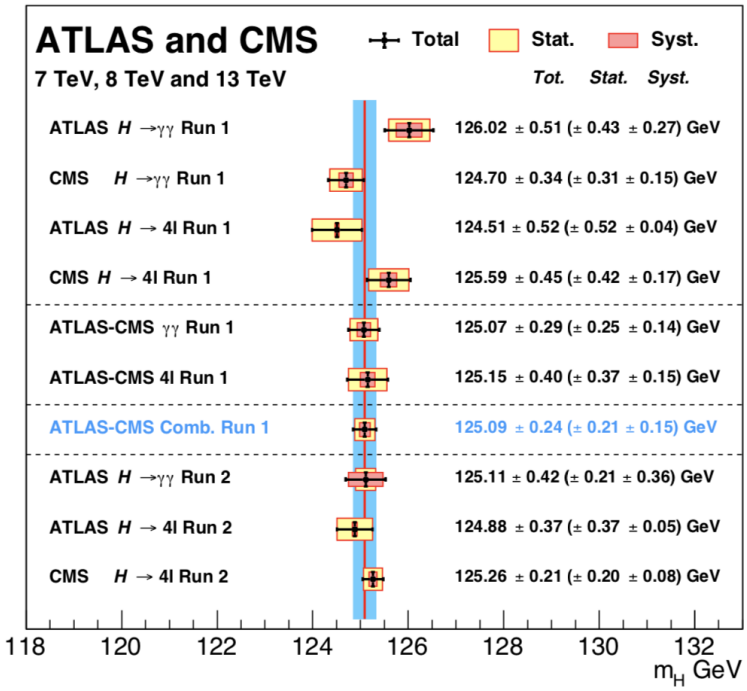


**Figure 1.6:** Summary of the CMS and ATLAS mass measurements in the $\gamma\gamma$ and ZZ channels in pp collisions during Run 1 and Run 2. (REF PDG19).

### 1.1.5 Status of the Higgs boson physics - from PDG19

"Conclusion summary from PDG"
Milestone measurements have been performed: (i) a clear observation of the Higgs boson decay to taus has been made by the CMS experiment; (ii) unambiguous evidence for the Higgs boson decay to a pair of b quarks was provided by both the ATLAS and CMS experiments; (iii) the ATLAS and CMS experiments have also provided evidence for the production of the Higgs boson through the $t\bar{t}$ H mechanism, thus yielding direct evidence for the Yukawa coupling of the Higgs boson to top quarks, with a strength compatible with that of the Standard Model. These and all other experimental measurements are consistent with the EWSB mechanism of the Standard Model.

Many extensions of the SM at higher energies call for an enlargement of the EWSB sector. Hence, direct searches for additional scalar states can provide valuable insights on the dynamics of the EWSB mechanism. The ATLAS and CMS experiments have searched for additional Higgs bosons in the Run 2 data, and imposed constraints in broad ranges of mass and couplings for various extended Higgs scenarios.

## 1.2 Physics Beyond the Standard Model

### 1.2.1 Shortcomings of the SM

Shortcomings of the SM [ The Standard Model is a very successful theory and its predictions have been verified over a wide range of energies. Among them, a particular importance has the discovery of the Higgs boson by the ATLAS and CMS collaborations in 2012 [**??**arie]. However, the SM has several shortcomings, as described below. (and this is the reason why a lot of different theories BSM have been created in the last years to extend it.)

- First of all, the SM is not a complete theory: it unifies only 3 of the 4 fundamental interactions, leaving aside the gravitation (described successfully by the theory of General Relativity).
  (da modificare : To combine the quantum theory of the SM with general relativity, a quantum theory of gravity is necessary, which could be obtained by adding a particle carrying the gravitational force, a graviton. This proves to be difficult because of the way the gravity interacts with the geometry of spacetime. The strength of the gravitational force is much lower than the ones from the other three fundamental forces. While those have a similar strength that shows an effect at the electroweak scale of O(100 GeV), the energy at which gravitational interactions become relevant is at the order of the Planck scale $E_P = 10^{19}$ GeV, which is defined by the Planck mass, $M_P = \sqrt{\frac{\hbar c}{G_N}}$, with $G_N$ being the gravitational constant. The huge difference between the electroweak scale and the Planck scale is also known as a hierarchy problem.)

- "Naturalness" of the theory : (The hierarchy problem implies that the mass of the Higgs boson should be of the order of the Planck scale. In order for the observed mass value to be 125 GeV, a fine-tuned cancellation of the bare mass and the contri- bution from Feynman diagrams loop corrections, both of O($10^{19}$ GeV), is necessary. )

- In the original formulation of the SM, neutrinos were strictly massless, but experimental evidences have established the existence of neutrino oscillations, i.e. transitions between the different neutrino flavors. This is an evidence for neutrino mixing and nonzero neutrino masses [**??** Vanf 1].
  (modifica: A mass term for the neutrinos can be added to the SM, but it is not clear if the small masses that the neutrinos must have can arise from the same electroweak symmetry breaking mechanisms than the masses for the other particles of the SM.)

- From astrophysical observations is known that the visible content of matter can only be approximately 5% of the total matter and energy content of our universe. Therefore, it has been hypothesized the existence of an unknown type of matter and energy, called *dark matter* and *dark energy*, which cannot be explained within the SM. The dark matter (25%) is assumed not to interact electromagnetically or by strong interactions, while the dark energy (70%) is thought to be responsible for the observed accelerated expansion of the universe.

- the CP-violating effects of the SM cannot explain the large difference between the amount of matter and anti-matter in the universe [1].

- the SM has a large number of free parameters:
  - 17 (EW theory) = 2 coupling constants ($g$, $g'$), 2 provided by Higgs mechanism ($m_{\rho'}$, $m_W$ (or $m_Z$) oppure mass and vacuum expectation value of the Higgs boson), 4 given by the Cabibbo-Kobayashi-Maskawa $V_{CKM}$ matrix (3 angles + 1 phase) and 9 coupling constants of the different fermions with the Higgs field, in order to obtain the fermion masses (3 charged leptons + 6 quarks).
  - 1 (QCD) = 1 coupling constant ($g_S$)
  Including also the neutrino oscillations, there are other 7 parameters to take into account: 3 neutrino masses and 4 parameters for the PMNS matrix.
  In total 25 parameters: all of them have been measured!

- ( da modificare: The SM coupling constants of the electromagnetic interaction, the weak interaction and the strong interaction have a similar value at an energy scale of O(1016 GeV). However, they do not converge to a single value as shown in Figure 1.1. In order to unify the coupling constants, an extension of the SM is necessary that changes the evolution above the electroweak scale.) Aggiungi immagine

(from all these considerations it is evident that there must be new physics at a scale beyond the electroweak scale. What is unknown, however, is the energy scale at which this new physics will manifest itself. It could be as high as the Planck scale, but this would mean that the hierarchy problem remains unsolved. Therefore, it is rather believed that there should be new physics at the TeV scale, at which a discovery with direct searches at the LHC could be possible.)

### 1.2.2 SM extensions

**Neutrino oscillations - by Wiki**

The so-called *neutrino oscillations* is the phenomenon whereby a neutrino created with a specific lepton family number ("lepton flavor": electron, muon, or tau) can later be measured to have a different lepton family number. This phenomenon was predicted by Bruno Pontecorvo in 1957 and it has been observed by a several experiments in several different contexts. it implies that the neutrino has a non-zero mass, which requires a modification to the Standard Model of particle physics.

The experimental discovery of neutrino oscillation, and thus neutrino mass, by the Super-Kamiokande Observatory and the Sudbury Neutrino Observatories was recognized with the 2015 Nobel Prize for Physics.

Neutrino oscillation arises from mixing between the flavor and mass eigenstates of neutrinos. That is, the three neutrino states that interact with the charged leptons in weak interactions are each a different superposition of the three (propagating) neutrino states of

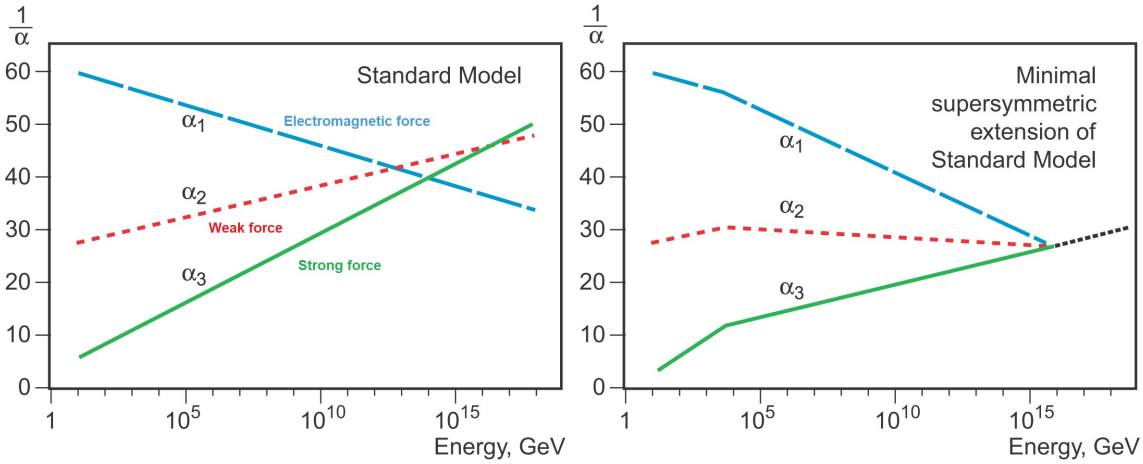


**Figure 2.7:** Evolution of the couplings $\alpha_i = \frac{g_i^2}{4\pi}$ as a function of the energy as predicted by the SM (on the left) and by the MSSM (on the right). The coupling constants of the strong weak and electromagnetic force are shown respectively in green, red and blue.

definite mass. Neutrinos are emitted and absorbed in weak processes in their flavor eigenstates[a] but travel as mass eigenstates. As a neutrino superposition propagates through space, the quantum mechanical phases of the three mass states advance at slightly different rates, due to the slight differences in their respective neutrino masses. This results in a changing superposition mixture of mass eigenstates as the neutrino travels. The electron flavor content of the neutrino will then continue to oscillate – as long as the quantum mechanical state maintains coherence. Since mass differences between neutrino flavors are small in comparison with long coherence lengths for neutrino oscillations, this microscopic quantum effect becomes observable over macroscopic distances.
In contrast, due to their larger masses, the charged leptons (electrons, muons, and tau leptons) have never been observed to oscillate.

The original Pontecorvo's idea was included in a quantitative theory developed by Maki, Nakagawa, and Sakata in 1962 and further elaborated by Pontecorvo in 1967 [15].

This theory successfully explained the deficit observed in solar neutrinos the year later.

In its simplest form the neutrino oscillation is expressed as a unitary transformation relating the flavor and mass eigenbasis and can be written as:

$$|\nu_\alpha\rangle = \sum_i U^*_{\alpha i} \, |\nu_i\rangle$$

$$|\nu_i\rangle = \sum_\alpha U_{\alpha i} \, |\nu_\alpha\rangle$$

where:

- $|\nu_\alpha\rangle$ is a neutrino with definite flavor $\alpha =$ e (electron), $\mu$ (muon) or $\tau$ (tauon),
- $|\nu_i\rangle$ is a neutrino with definite mass $m_i, i = 1, 2, 3$.

$U_{\alpha i}$ is the Pontecorvo–Maki–Nakagawa–Sakata matrix (PMNS matrix), which is the analogue of the CKM matrix describing the mixing of quarks. It is a 3×3 matrix given by:
$\begin{pmatrix} U_{e_1} & U_{e_2} & U_{e_3} \\ U_{\mu_1} & U_{\mu_2} & U_{\mu_3} \\ U_{\tau_1} & U_{\tau_2} & U_{\tau_3} \end{pmatrix}$

Bla bla bla, se vuoi approfondisci ... (parametrizzazione matrice e risultati sperimentali up to now)

$$\begin{pmatrix} \nu_e \\ \nu_\mu \\ \nu_\tau \end{pmatrix} = \begin{pmatrix} U_{e_1} & U_{e_2} & U_{e_3} \\ U_{\mu_1} & U_{\mu_2} & U_{\mu_3} \\ U_{\tau_1} & U_{\tau_2} & U_{\tau_3} \end{pmatrix} \begin{pmatrix} \nu_e \\ \nu_\mu \\ \nu_\tau \end{pmatrix} \tag{2.7}$$

## 1.3 Lepton Flavor Violation (LFV)

### 1.3.1 LFV in SM

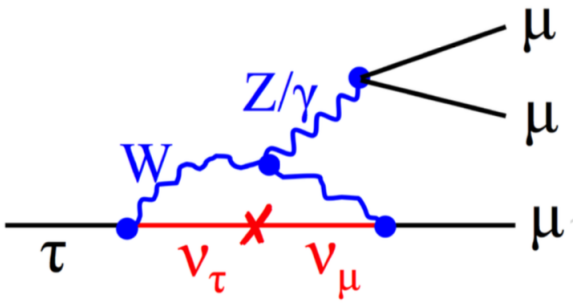


**Figure 3.8:** FD/SM.

### 1.3.2 LFV in BSM

#### Supersymmetric Model with R-Parity Violation

The discrete R-parity has been introduced into Supersymmetry [18] because ...

It is defined as:

$$R_p = (-1)^R = \begin{cases} +1 & \text{for SM particles } (R-even) \\ -1 & \text{for SUSY particles } (R-odd) \end{cases} \tag{3.8}$$

where $R$ is defined as $R = 3B + L + 2S$ where $B$ and $L$ are respectively the baryon and the lepton numbers, while $S$ is the spin of the particle.

This parity guarantees that the lightest supersymmetric particle is stable and therefore it is a good candidate for dark matter.

In supersymmetric models with R-parity violation which are still possible with respect to the present experimental bounds, an additional non-diagonal Yukawa coupling between the charged leptons and sneutrinos allows lepton flavour violation in the charged lepton sector [19].
The contributing Feynman diagram to the decay $\tau \to \mu\mu$ is depicted in Fig. 3.9.

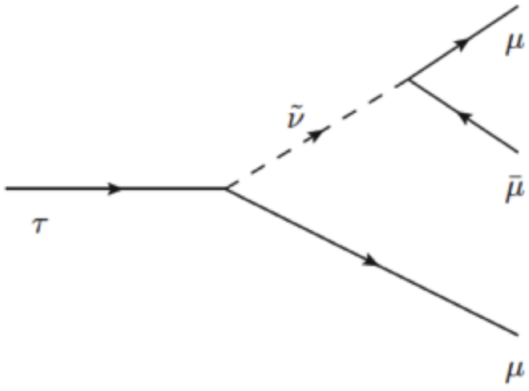


**Figure 3.9:** FD/BSM.

### 1.3.3 Analysis theorical intro

In nature there are no known symmetries that would forbid leptons decays in which the flavor is not conserved. These lepton-flavor violation (LFV) decays can be of the kind: $l \to l'\gamma$, $l \to 3l'$ and $l \to 2\mu e/2e\mu$ (where $l$ and $l'$ are leptons (e, $\mu$, $\tau$) with different flavor). Among these possible decays, the second one was chosen to be searched for in the work of this thesis. In particular, the analysis I have performed had the purpose to search for $\tau \to 3\mu$ decays. Actually, in the SM with the neutrino oscillations, such kind of decays are possible and they are described in terms of Feynman diagrams as shown in Fig. 3.8.

However, this kind of decay is predicted with a small branching fraction: $\mathcal{B}(\tau \to 3\mu \sim \mathcal{O}(10^{-14})$. [ref. AN] In present day experiment a so low BR is not accessible! On the other hand, several theories that aim to extend the SM, called "Beyond Standard Model" (BSM) theories, allow these LFV decays with a BR which is enhanced of several orders of magnitude, resulting in cross section values which can be tested with current experiments[ref. AN]. An example of the decay mechanisms predicted for this channel by one BSM is shown in Fig. 3.9.

The chosen of this particular decay channel to investigate this kind of violation is motivated by several reasons:

1. Other kind of LFV decays are expected to be extremely suppressed, with a BR many orders of magnitude smaller! For example: $\mathcal{B}(\tau \to \mu\gamma \sim \mathcal{O}(10^{-40})$. [ref. AN]

2. LHC is a $\tau$ factory! the expected inclusive production cross section for pp collisions is about $2 \times 10^{11}$ fb . [ref. AN]

3. CMS is brilliant in detecting muons

4. The enhancements predicted by BSMs may be larger for heavier-flavor lepton [ref. AN]

The search for this kind of decay has been already performed in the last years by different experiments, but no signal has never been observed, leading to the determination of an upper limit value for the BR of the process. The best experimental value set for this upper limit, up to now, is the one obtained by Belle experiment [ref. AN] : $\mathcal{B}(\tau \to 3\mu \ \leq \ 2.1 \cdot 10^{-8}$ at 90% confidence level [20]. A similar result was obtained by BaBar, another experiment operating, as Belle, at an $e^+e^-$ collider and now decommissioned, that set the limit at $3.3 \cdot 10^{-8}$ [21].

Also LHC experiments have looked for this decay, with the following results:

- LHCb: 4.6 $\times 10^{-8}$ [22],
- ATLAS: 3.8 $\times 10^{-7}$ [23]
- CMS (only 2016 data - 33 $fb^{-1}$) : 8.8 $\times 10^{-8}$ - [ref. AN]

# Chapter 2

# The CMS experiment at LHC

# Chapter 3

# Events reconstruction in CMS

# Chapter 4

# Analysis

(This analysis was performed in CMS on the 2016 data: int. lumi of 33 $fb^{-1}$ of pp collision at center of mass energy $\sqrt{s} = 13$ TeV. No signal has been observed, putting an upper limit on the branching fraction of the tau lepton decaying in 3 muons $\mathcal{B}(\tau \to 3\mu)$ of 8.8 $\times 10^{-8}$ at 90% confidence level. -¿ Si può citare il PAS ?)

## 4.1 Preliminary considerations

### 4.1.1 Production of $\tau$ leptons at LHC

As said previously, the LHC collider is a $\tau$ factory! These leptons can be produced in different processes, leading to an estimation of the total INCLUSIVE number of them of $sim$ $2 \times 10^{11}$ fb.

( qui ci sarebbe la tabella con i vari processi e il relativo numero di leptoni ... quella della Florida è riferita alla luminosità del 2016)!

In pp collisions, $\tau$ leptons are produced mainly from hadrons containing c or b quarks (in particular from D and B mesons and only rarely from c/b-baryons) and from the decays of W and Z bosons: $W \to \tau\nu_\tau$ and $Z \to \tau^+\tau^-$.

Tau leptons can be originated also by B meson decaying in D mesons that in turn decays in tau lepton + neutrino. These "indirect" decays can be distinguished from the "direct/prompt" ones (from directly produced D mesons) because they are characterized by larger transverse momenta and displaced vertices.

The expected inclusive number of $\tau$ coming from different processes are reported in Tab. 4.1.

The relative $\tau$ yields are listed in Tab. 4.2.

| Process1 | Process2 | N. of $\tau$ for L =? |
|---|---|---|
| $pp \to c\bar{c} + ...$ | $D \to \tau\nu_\tau$<br>(95% $D_s$, 5% $D^\pm$) | 000 |
| $pp \to b\bar{b} + ...$ | $B \to \tau\nu_\tau + ...$<br>(44% $B^\pm$, 45% $B^0$, 11% $B_s^0$)<br>$B \to D(\tau\nu_\tau) + ...$<br>(98% $D_s$, 2% $D^\pm$) | 000<br><br>000 |
| $pp \to W + ...$<br>$pp \to Z + ...$ | $W \to \tau\nu_\tau + ...$<br>$Z + ... \to \tau\tau + ...$ | 000<br>000 |

**Table 4.1:** List of processes from which $\tau$ leptons are produced, with their corresponding expected inclusive number for L = ? // The charge-conjugated states are included.

| Mother meson | Quark composition | Meson mass (GeV) | Relative $\tau$ yield |
|---|---|---|---|
| $D_s$ | $c\bar{s}$ | 1.97 | 72% |
| $D^+$ | $c\bar{d}$ | 1.87 | 3% |
| $B^+$ | $\bar{b}u$ | 5.28 | 11% |
| $B^0$ | $\bar{b}d$ | 5.28 | 11% |
| $B_s$ | $\bar{b}s$ | 5.37 | 3% |

**Table 4.2:** List of mesons from which $\tau$ are produced with the relative tau yields. The charge-conjugated states are included.

### 4.1.2 Signal acceptance

## 4.2 Outline: search strategy

## 4.3 Data and MonteCarlo samples

### 4.3.1 Datasets

For the analysis described in this thesis, I have used data collected by CMS in pp collisions at a center of mass energy $\sqrt{s} = 13$ TeV during Run II in the whole 2017.
These datasets are listed in Tab. 4.3.
They correspond to a total integrated luminosity: $\mathcal{L} = 41.49\ fb^{-1}$.

| 2017 Datasets | Run range | Integr. Luminosity ($fb^{-1}$) |
|---|---|---|
| /DoubleMuonLowMass/Run2017B-17Nov2017-v1/AOD | 000 | 4.79 |
| /DoubleMuonLowMass/Run2017C-17Nov2017-v1/AOD | 000 | 9.63 |
| /DoubleMuonLowMass/Run2017D-17Nov2017-v1/AOD | 000 | 4.25 |
| /DoubleMuonLowMass/Run2017E-17Nov2017-v1/AOD | 000 | 9.30 |
| /DoubleMuonLowMass/Run2017F-17Nov2017-v1/AOD | 000 | 13.52 |
| Whole 2017 data | 000 | 41.49 |

**Table 4.3:** Datasets of the whole 2017 data-taking that have been used for the analysis described in this thesis.

The json file used for data processing is:
Collisions17/13TeV/ReReco/Cert$_2$94927 − 306462$_1$3TeV$_E$OY2017ReReco$_C$ollisions17$_J$SON$_v$1.txt.

### 4.3.2 MonteCarlo samples

The MC samples used in this analysis are listed in Tab. 4.4.

| Simulated process | MC Dataset name |
|---|---|
| $D_s \to \tau\nu_\tau \to 3\mu\ \nu_\tau$ | /DsToTau$_T$o3Mu$_M$uFilter$_T$uneCUEP8M1$_1$3TeV − pythia8/RunIIFall17DRPremix − |
| $B^0 \to \tau\nu_\tau \to 3\mu\ \nu_\tau$ | /BuToTau$_T$o3Mu$_M$uFilter$_T$uneCUEP8M1$_1$3TeV − pythia8/RunIISummer16DR80Premix − PUMori |
| $B^\pm \to \tau\nu_\tau \to 3\mu\ \nu_\tau$ | /BdToTau$_T$o3Mu$_M$uFilter$_T$uneCUEP8M1$_1$3TeV − pythia8/RunIISummer16DR80PremixPUMorio |
| $D_s \to \phi\pi \to 2\mu\ \pi$ | /DsPhiPi/fsimone − crab$_c$rab$_D$sPhiPi$_1$3TeV$_R$ECO − c3763c515b5d7d94a8 |

**Table 4.4:** MC samples used for the analysis described in this thesis.

The branching fractions of the B and D mesons decays are listed in Tab. 4.5.

| Process | Branching ratio(BR) | Reference |
|---|---|---|
| $D_s \to \tau\nu_\tau$ | 5.48 ± 0.23% | PDG [73] |
| $B^+ \to \tau\nu_\tau D_0^*$ | 2.7 ± 0.3% | PDG [73] |
| other$B^+ \to \tau\nu_\tau X$ | 0.7% | PYTHIA [70] |
| $B^0 \to \tau\nu_\tau D^{+*}$ | 2.7 ± 0.3% | PDG [73] |
| other$B^0 \to \tau\nu_\tau X$ | 0.7% | PYTHIA [70] |
| $B^+ \to D_s X$ | 9.0 ± 1.5% | PDG [73] |
| $B^0 \to D_s X$ | 10.3 ± 2.1% | PDG [73] |
| $D_s \to \phi(\mu\mu)\pi$ | 1.3(± 0.1 $\cdot 10^{-5}$) | PDG [73] |

**Table 4.5:** MC samples used for the analysis described in this thesis.

## 4.4 Event selection

| | Signal | | Data |
|---|---|---|---|
| | $D_s \to \tau\nu_\tau$ | $B^\pm/B^0 \to \tau$... | |
| Produced in pp collisions | 000 | 000 | |
| (with three muons in fiducial volume) | 000 | 000 | |
| L1/HLT trigger | 000 | 000 | |
| At least 3 GlobalMuon ($p_T$ > 2 GeV) | 000 | 000 | 000 |
| Trimuon candidate selection | 000 | 000 | 000 |

**Table 4.6:** Bla Bla

The PRE-selections applied to choose the interesting (DsTau3Mu) events are the following:

1. Fired HLT : at least one HLT path among
   - HLT_DoubleMu3_Trk_Tau3mu_v∗

- HLT_DoubleMu3_TkMu_DsTau3Mu_v*
- HLT_DoubleMu3_Trk_Tau3mu_NoL1Mass_v*

2. At least 3 muons with :
   - $p_T > 0.5$
   - $|\eta| < 2.4$
   - innerTrack().isNonnull
   - charge $\neq 0$
   - innerTrack().hitPattern().numberOfValidPixelHits()$> 0$
3. At least 1 triplet with |charge| = 1

The selections applied on the triplets to choose the interesting (DsTau3Mu) ones are the following:

1. The $\chi^2$ of the triplet vertex is in (0-15)
2. The 3 possible pairs of mu of the triplet have $\Delta R < 0.8$
3. The 3 possible pairs of mu of the triplet have $|\Delta Z| < 0.5$
4. VETO on mass of o.s. muons of the triplet compatible with $\phi$ meson
5. VETO on mass of o.s. muons of the triplet compatible with $\omega$ meson
6. Mass window ??
7. L1 ???
8. trigger matching requirements

If more than one triplet per event survives, it's chosen the one with the best (min) $\chi^2$ value.

## 4.5 Signal Normalization

### 4.5.1 Events triggered by DoubleMu L1 seeds

$$N_{sig(D)} = \mathcal{L}\ \sigma(pp \to D_s)\ \mathcal{B}(D_s \to \tau\nu_\tau)\ \mathcal{B}(\tau \to 3\mu)\ \mathcal{A}_{3\mu(D)}\ \epsilon^{3\mu}_{reco}\ \epsilon^{2\mu}_{trig} \tag{5.1}$$

$$N = \mathcal{L}\ \sigma(pp \to D_s)\ \mathcal{B}(D_s \to \phi\pi \to \mu\mu\pi)\ \mathcal{A}_{2\mu\pi}\ \epsilon^{2\mu\pi}_{reco}\ \epsilon^{2\mu}_{trig} \tag{5.2}$$

$$N_{sig(D)} = N\ \cdot \frac{\mathcal{B}(D_s \to \tau\nu_\tau)}{\mathcal{B}(D_s \to \phi\pi \to \mu\mu\pi)}\ \frac{\mathcal{A}_{3\mu(D)}}{\mathcal{A}_{2\mu\pi}}\ \frac{\epsilon^{3\mu}_{reco}}{\epsilon^{2\mu\pi}_{reco}}\ \mathcal{B}(\tau \to 3\mu) \tag{5.3}$$

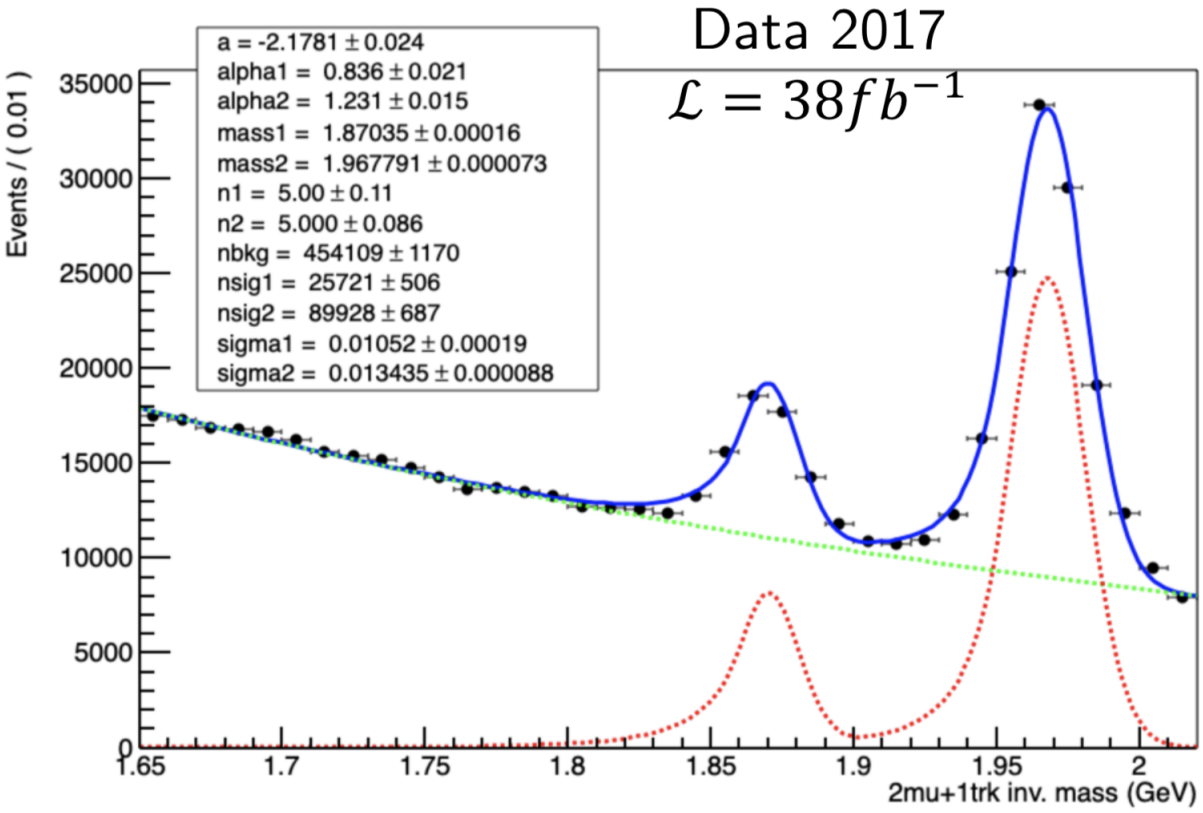


**Figure 5.1:** NDs-total.

| Run | Fitted $D_s \to \phi(\mu\mu)\pi$ yields ($fb^{-1}$) | Data/MC ratio |
|---|---|---|
| 2017 B | 000 | 000 |
| 2017 C | 000 | 000 |
| 2017 D | 000 | 000 |
| 2017 E | 000 | 000 |
| 2017 F | 000 | 000 |
| Whole 2017 | 000 | 000 |

**Table 4.7:** Bla Bla

### 4.5.2 B/D ratio

$$N_{sig(B)} = \mathcal{L}\ \sigma(pp \to B)\ \mathcal{B}(B \to \tau + ...)\ \mathcal{B}(\tau \to 3\mu)\ \mathcal{A}_{3\mu(B)}\ \epsilon^{3\mu}_{reco}\ \epsilon^{2\mu}_{trig} \tag{5.4}$$

$$f\ =\ \frac{\sigma(pp \to B)\ \mathcal{B}(B \to D_s + ...)}{\sigma(pp \to D_s)} \tag{5.5}$$

$$N_{sig(B)} = N \cdot\ f \cdot\ \frac{\mathcal{B}(B \to \tau + ...)}{\mathcal{B}(D_s \to \phi\pi \to \mu\mu\pi)\ \mathcal{B}(B \to D_s + ...)}\ \frac{\mathcal{A}_{3\mu(B)}}{\mathcal{A}_{2\mu\pi}}\ \frac{\epsilon^{3\mu}_{reco}}{\epsilon^{2\mu\pi}_{reco}}\ \mathcal{B}(\tau \to 3\mu) \tag{5.6}$$

### 4.5.3 Control channel

MC validation with $D_s \to \phi(\mu\mu)\pi$.

PRE-selections applied on the events:

1. Fired HLT path: $HLT\_DoubleMu3\_Trk\_Tau3mu\_v*$
2. at least 1 triplet with:
   - 2 muons with:
     - $p_T > 0.5$
     - $|\eta| < 2.4$
     - innerTrack().isNonnull
     - charge $\neq 0$
     - innerTrack().hitPattern().numberOfValidPixelHits() $> 0$
   - 1 track with:
     - $p_T > 2$
     - $|\eta| < 2.4$
     - charge $\neq 0$
     - hitPattern().trackerLayersWithMeasurement() $> 5$
     - hitPattern().pixelLayersWithMeasurement() $\geq 1$
3. the triplet must have:
   - mass in (0.5 - 10) GeV
   - |charge| = 1

The selections applied on the triplets are:

1. L1 trigger trigger fired: $L1\_DoubleMu0er1p5\_SQ\_OS\_dR\_Max1p4$
2. the 2 muons are global and different from the track
3. the $\chi^2$ of the triplet vertex is in [0,15]
4. the 2 muons have opposite charge
5. the 2 muons invariant mass is in [1, 1.04] GeV
6. the longitudinal IP $< 20$ cm and the transverse IP $< 0.3$ cm
7. trigger matching requirements:
   - Mu01_dRtriggerMatch $< 0.03$
   - Mu02_dRtriggerMatch $< 0.03$
   - Tr_dRtriggerMatch $< 0.03$

If more than one triplet per event survives, it's chosen the one with the best (min) $\chi^2$ value.

## 4.6 Multivariate Analysis (MVA)

### 4.6.1 Introduction to MVA: why to use it?

The Multivariate analysis has assumed progressively a central role in high energy physics searches [75]. In this field, this kind of analysis aims to exploit as much information as possible from the characteristics of each event in order to distinguish between event types (eg. signal and background).
In order to understand how this analysis works and which are the improvements in using it with respect to "traditional" analysis performed by successive cuts, let's look at the scatter plots in Fig. 6.2. They show the distribution of two variables $x_1$ and $x_2$ which represent two out of a potentially large number of quantities measured for each event, with different decision boundaries (cuts, lineary boundary, non linear boundary). The signal events are indicated with blue circles while the red triangles represent the background ones.

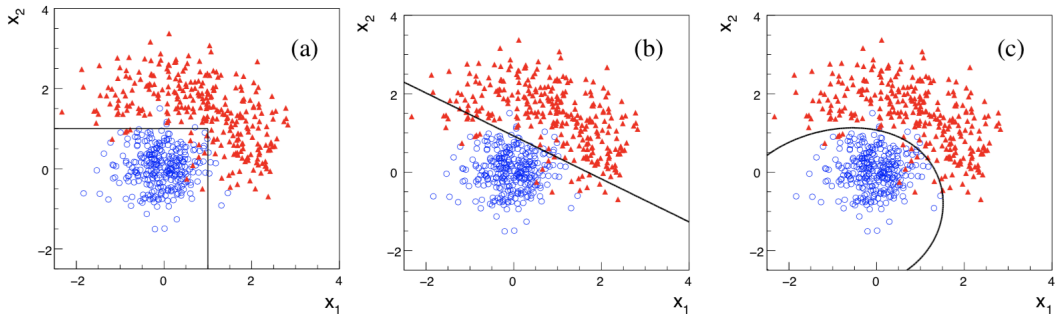


**Figure 6.2:** Scatter plots of two variables corresponding to two hypotheses: signal (blue) and background (red). Event selection could be based, e.g., on (a) cuts, (b) a linear boundary, (c) a nonlinear boundary. [75].

It is evident that rectangular and diagonal cuts are not as good as nonlinear boundaries in classifying the events. In general, the best decision boundary is a surface in the n-dimensional space of input variables, which can be represented by an equation of the form $y(\boldsymbol{x}) = y_{cut}$, where $y_{cut}$ is some constant. Events are classified as signal if they are on one side of the boundary, e.g., $y(\boldsymbol{x}) \leq y_{cut}$, could represent the acceptance region and $y(\boldsymbol{x}) > y_{cut}$ could be the rejection region.
- oppure utilizzo come "scalar test" statistics (vedi 14-15 Cowan per more details )

### 4.6.2 Boosted Decision Tree (BDT)

#### Decision Tree

A decision tree is a binary tree structured classifier, defined by a collection of successive cuts on the set of input variables. It is schematically represented in Fig. 6.3.

Starting from the entire sample of training events in the root node, out of all of the

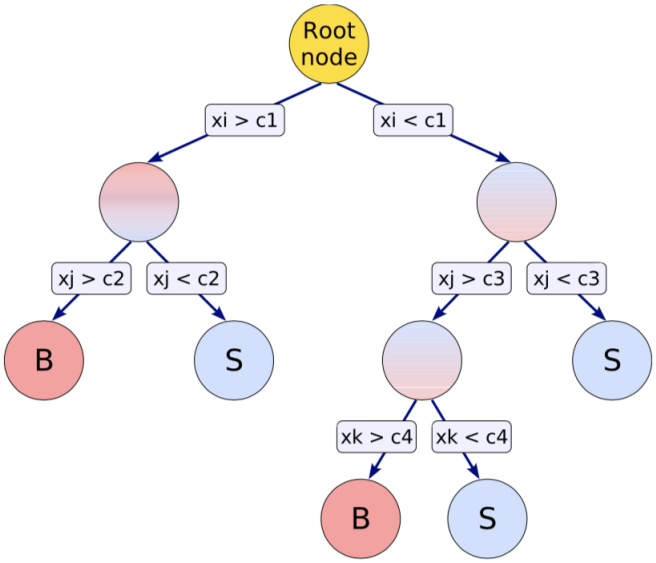


**Figure 6.3:** Scheme of a decision tree. A sequence of binary splits using the discriminating variables xi is applied to the data, starting from the root node. Each split uses the variable that, at that node, discriminates in the best way signal(S) and background(B). The leaf nodes at the bottom end of the tree are labeled (S or B) depending on the majority of events that end up in the respective nodes [76].

possible input variables, one finds the ones that provide the best separation between signal and background by use of a single cut. Then, repeated left/right (yes/no) decisions are taken on one single variable at a time until a stop criterion is fulfilled.
In this way, the phase space is split into many regions that are eventually classified as signal or background, depending on the majority of training events that end up in the final leaf node.
Therefore, the difference of this classifier, with respect to the case of rectangular cuts, is that whereas a cut-based analysis is able to select only one hypercube as region of phase space, the decision tree is able to split the phase space into a large number of hypercubes, each of which is identified as either "signal-like" or "background-like". For classification trees, the path down the tree to each leaf node represents an individual cut sequence that selects signal or background depending on the type of the leaf node.

A shortcoming of decision trees is their instability with respect to statistical fluctuations in the training sample from which the tree structure is derived.
This problem can be overcome by using a Boosted Decision Tree.

### Boosting the tree...

The boosting of a decision tree extends this concept from one tree to several trees, which form a *forest*.
The trees are derived from the same training ensemble by reweighting events (procedure

called "boosting"), and are finally combined into a single classifier which is given by an average of the individual decision trees. This boosting increases the statistical stability of the classifier and is able to drastically improve the separation performance compared to a single decision tree.
(In many cases, the boosting performs best if applied to trees that, taken individually, have not much classification power. These so called "weak classifiers" are small trees, limited in growth to a typical tree depth of as small as two, depending on the how much interaction there is between the different input variables. By limiting the tree depth during the tree building process (training), the tendency of overtraining for simple decision trees which are typically grown to a large depth and then pruned, is almost completely eliminated.)
A number of boosting algorithms have been developed, and these differ primarily in the rule used to update the weights; the one employed in the BDT used in this analysis is the so-called *AdaBoost* (adaptive boost), which is explained in detail in [64].

**Training a decision tree**

(ridurre: in molte parti è una ripetizione di quanto già detto! Accorpare al precedente!)

The training of a decision tree is the process that defines the splitting criteria for each node. It starts with the root node, where an initial splitting criterion for the full training sample is determined. The split results in two subsets of training events that each go through the same algorithm of determining the next splitting iteration. This procedure is repeated until the whole tree is built. At each node, the split is determined by finding the variable and corresponding cut value that provides the best separation between signal and background. The node splitting stops once it has reached the minimum number of events which is specified in the BDT configuration (option nEventsMin). The leaf nodes are classified as signal or background according to the class the majority of events belongs to. A variety of separation criteria can be configured to assess the performance of a variable and a specific cut requirement. Because a cut that selects predominantly background is as valuable as one that selects signal, the criteria are symmetric with respect to the event classes. All separation criteria have a maximum where the samples are fully mixed, i.e., at purity p = 0.5, and fall off to zero when the sample consists of one event class only.

Since the splitting criterion is always a cut on a single variable, the training procedure selects the variable and cut value that optimises the increase in the separation index between the parent node and the sum of the indices of the two daughter nodes, weighted by their relative fraction of events. The cut values are optimised by scanning over the variable range with a granularity that is set via the option nCuts.

PROVARE!!! The default value of nCuts=20 proved to be a good compromise between computing time and step size. Finer stepping values did not increase noticeably the performance of the BDTs. However, a truly optimal cut, given the training sample, is determined by setting nCuts=-1. This invokes an algorithm that tests all possible cuts on the training sample and finds the best one.

### Variable ranking

A ranking of the BDT input variables is derived by counting how often the variables are used to split decision tree nodes, and by weighting each split occurrence by the separation gain-squared it has achieved and by the number of events in the node.
This measure of the variable importance can be used for a single decision tree as well as for a forest.

### Performance

PUNTO a FAVORE: Decision trees are also insensitive to the inclusion of poorly discriminating input variables (which is not the case of neural networks, for example).

Boosted decision trees have become increasingly popular in particle physics in recent years. One of their advantages is that they are relatively insensitive to the number of input variables used in the data vector x. Components that provide little or no separation between signal and background are rarely chosen as for the cut that provides separation, i.e., to split the tree, and thus they are effectively ignored. Decision trees have no difficulty in dealing with different types of data; these can be real, integer, or they can simply be labels for which there is no natural ordering (categorical data). Furthermore, boosted decision trees are surprisingly insensitive to overtraining. That is, although the error rate on the test sample will not decrease to zero as one increases the number of boosting iterations (as is the case for the training sample), it tends not to increase. Further discussion of this point can be found in [77]. – copia-e-incolla- END

- TMVA

The Toolkit for Multivariate Analysis (TMVA) provides a ROOT-integrated [76] environment for the application of multivariate classification techniques.
All TMVA techniques belong to the family of *supervised learning* algorithms. They make use of training events, for which the desired output is known, to determine the mapping function that describes a decision boundary (classification). This function can contain various degrees of approximations and may be a single global function, or a set of local models.
A typical TMVA classification consists of two independent phases: the *training phase*, where the multivariate methods are trained, tested and evaluated, and an *application phase*, where the chosen methods are applied to the concrete classification or regression problem they have been trained for.

| Input variable | Importance |
|---|---|
| var | 000 |
| var | 000 |
| var | 000 |
| var | 000 |
| var | 000 |
| var | 000 |
| var | 000 |
| var | 000 |
| var | 000 |
| var | 000 |

**Table 4.8:** Bla Bla

| Parameter | Setting (default) |
|---|---|
| NTrees | 800 |
| nCuts | 20 |
| MaxDepth | 3 |
| BoostType | AdaBoost |

**Table 4.9:** Bla Bla

### 4.6.3 BDT training

### 4.6.4 Event categorization

## 4.7 Evaluation of systematics

Bla Bla [78]

| Source of uncertainty | Yield | Shape |
|---|---|---|
| Uncertainty on $D_s$ normalization [ 3.5% ] | 000 | |
| Uncertainty on measuring f (B/D ratio) [ 10% ] | 000 | |
| Uncertainty on n. of events triggered by trimuon trigger [ 12% ] | 000 | |
| Relative uncertainty in $\mathcal{B}(D_s \to \phi\pi \to \mu\mu\pi)$ [ 8% ] | 000 | |
| Relative uncertainty in $\mathcal{B}(D_s \to \mu\nu)$ [ 4% ] | 000 | |
| Relative uncertainty in $\mathcal{B}(B \to D_s + ...)$ [ 16% ] | 000 | |
| Relative uncertainty in $\mathcal{B}(B \to \tau + ...)$ [ 11% ] | 000 | |
| Uncertainty on the ratio of acceptances $\mathcal{A}_{sig}$ / $\mathcal{A}_{2\mu\pi}$ [ 1% ] | 000 | |
| Muon reconstruction efficiency [ 1.5% ] | 000 | |
| BDT cut efficiency [ 5% ] | 000 | |
| Muon momentum scale uncertainty [ 0.2% ] | - | yes |
| Muon momentum resolution uncertainty [ 10% ] | - | yes |

**Table 4.10:** Bla Bla

## 4.8 Results

$$q_\mu = -2\ \ln\ \frac{\mathcal{L}\ (\text{obs}|\ \mu \cdot \text{s} + \text{b},\ \hat{\theta_\mu})}{\mathcal{L}\ (\text{obs}|\ \hat{\mu} \cdot \text{s} + \text{b},\ \hat{\theta})} \tag{8.7}$$

$$\mathcal{L}(\text{data}|\ \mu\text{s} + \text{b})\ \sim\ e^{-(\mu S+B)}\ \prod_i \mathcal{P}(\text{x}_\text{i}|\ \mu\text{s} + \text{b}) \tag{8.8}$$

$$\text{CL}_\text{s}\ =\ \frac{\text{P}\ (\text{q}_\mu \geq \text{q}_\mu^{\text{obs}}\ |\mu \cdot\ \text{s} + \text{b})}{\text{P}\ (\text{q}_\mu \geq \text{q}_\mu^{\text{obs}}\ |\ \text{b})} \leq 0.1 \tag{8.9}$$

| | Signal | | Background | |
|---|---|---|---|---|
| | sub-category 1 | sub-category 2 | sub-category 1 | sub-category 2 |
| Category A | 000 | 000 | 000 | 000 |
| Category B | 000 | 000 | 000 | 000 |
| Category C | 000 | 000 | 000 | 000 |

**Table 4.11:** Bla Bla

# Bibliography


[1] Otto Nachtmann, *"Elementary Particle Physics. Concepts and Phenomena"*, Springer-Verlag, Berlin Heidelberg 1990.

[2] Sheldon L. Glashow, *"Partial-symmetries of weak interactions"*, Nucl. Phys. 22, 579–588 (1961), doi:10.1016/0029-5582(61)90469-2.

[3] UA1 Collaboration, *"Experimental observation of isolated large transverse energy electrons with associated missing energy at $\sqrt{s}$=540 GeV"*, Phys.Lett. B122 (1983)103-116, doi: 10.1016/0370-2693(83)91177-2.

[4] UA1 Collaboration, *"Experimental observation of lepton pairs of invariant mass around 95 GeV/$c^2$ at the CERN SPS collider"*, Phys.Lett. B126 (1983) 398-410, doi: 10.1016/0370-2693(83)90188-0.

[5] Peter W. Higgs, *"Broken Symmetries, Massless Particles and Gauge Fields"*, Phys. Lett. 12, 132-133 (1964), doi:10.1016/0031-9163(64)91136-9.

[6] François Englert and Robert Brout, *"Broken Symmetry and the Mass of Gauge Vector Mesons"*, Phys. Rev. Lett. 13, 321-323 (1964), doi:10.1103/PhysRevLett.13.321.

[7] Peter W. Higgs, *"Broken Symmetries and the Masses of Gauge Bosons"*, Phys. Rev. Lett. 13, 508-509 (1964), doi:10.1103/PhysRevLett.13.508.

[8] Gerald S. Guralnik, Carl R. Hagen and Thomas W. Kibble, *"Global Conservation Laws and Massless Particles"*, Phys. Rev. Lett. 13, 585-587 (1964), hrefhttps://journals.aps.org/prl/abstract/10.1103/PhysRevLett.13.585doi:10.1103/PhysRevLett.13.5

[9] ATLAS Collaboration, *"Observation of a new particle in the search for the Standard Model Higgs boson with the ATLAS detector at the LHC"*, Phys. Lett. B 716 (2012) 1, doi:10.1016/j.physletb.2012.08.020, arXiv:1207.7214.

[10] CMS Collaboration, *"Observation of a new boson at a mass of 125 GeV with the CMS experiment at the LHC"*, Phys. Lett. B 716 (2012) 30, doi:10.1016/j.physletb.2012.08.021, arXiv:1207.7235.

[11] CMS Collaboration, *"Measurements of properties of the Higgs boson in the four-lepton final state in proton-proton collisions at $\sqrt{s}$ = 13 TeV"*, CMS-PAS-

HIG-19-001, http://cms-results.web.cern.ch/cms-results/public-results/preliminary-results/HIG-19-001/index.html.

[12] ATLAS Collaboration, *"Measurements of the Higgs boson inclusive, differential and production cross sections in the 4l decay channel at $\sqrt{s}$ = 13 TeV with the ATLAS detector"*, ATLAS-CONF-2019-025, http://cds.cern.ch/record/2682107/files/ATLAS-CONF-2019-025.pdf?version=2.

[13] CMS Collaboration, *"Measurements of Higgs boson production via gluon fusion and vector boson fusion in the diphoton decay channel at $\sqrt{s}$ 13 TeV"*, CMS-PAS-HIG-18-029,http://cms-results.web.cern.ch/cms-results/public-results/preliminary-results/HIG-18-029/index.html.

[14] ATLAS Collaboration, *"Measurements and interpretations of the Higgs-boson fiducial cross sections in the diphotons decay channel using 139 $fb^{-1}$ of pp collision data at $\sqrt{s}$ = 13 TeV with the ATLAS detector"*, ATLAS-CONF-2019-029, http://cds.cern.ch/record/2682800/files/ATLAS-CONF-2019-029.pdf?version=1.

[15] B. Pontecorvo, *"Neutrino Experiments and the Problem of Conservation of Leptonic Charge"*, Zh. Eksp. Teor. Fiz. 53: 1717–1725 (May 1968), http://www.jetp.ac.ru/cgi-bin/dn/e_026_05_0984.pdf.

[16]

[17] M. Giffels thesis

[18] R. Barbier et al., *"R-parity violating supersymmetry"*, Physics Reports, 420 (2005), 1, doi:10.1016/j.physrep.2005.08.006, arXiv:hep-ph/0406039.

[19] M. Giffels, J. Kallarackal, M. Kramer, B. O'Leary and A. Stahl, *"The lepton-flavour violating decay $\tau \to \mu\mu$ at the LHC"*, Phys.Rev.D77:073010,2008, doi:10.1103/PhysRevD.77.073010, arXiv:0802.0049.

[20] Belle Collaboration, *"Search for Lepton Flavor Violating Tau Decays into Three Leptons with 719 Million Produced Tau+Tau- Pairs"*, Phys. Lett. B 687 (2010) 139, doi:10.1016/j.physletb.2010.03.037, arXiv:1001.3221.

[21] BaBar Collaboration, *"Limits on tau Lepton-Flavor Violating Decays in three charged leptons"*, Phys. Rev. D 81 (2010) 111101, doi:10.1103/PhysRevD.81.111101, arXiv:1002.4550.

[22] LHCb Collaboration, *"Search for the lepton flavour violating decay $\tau^- \to \mu^-\mu^+\mu^-$"*, JHEP 02 (2015) 121, doi:10.1007/JHEP02(2015)121, arXiv:1409.8548.

[23] ATLAS Collaboration, *"Probing lepton flavour violation via neutrinoless $\tau \to 3\mu$ decays with the ATLAS detector"*, arXiv:1601.03567.

[24] L. Evans and P. Bryant, *"LHC Machine"*, JINST 3 (2008) S08001, doi:10.1088/1748-0221/3/08/S08001.

[25] *"The Large Electron-Positron Collider"*, http://cds.cern.ch/record/1997351, July2012.

[26] ATLAS Collaboration, *"The ATLAS Experiment at the CERN Large Hadron Collider"*, JINST 3 (2008) S08003, doi:10.1088/1748-0221/3/08/S08003.

[27] CMS Collaboration, *"The CMS experiment at the CERN LHC"*, JINST 3 (2008) S08004, doi:10.1088/1748-0221/3/08/S08004.

[28] LHCb Collaboration, *"The LHCb Detector at the LHC"*, JINST 3 (2008) S08005, doi:10.1088/1748-0221/3/08/S08005.

[29] ALICE Collaboration, *"The ALICE experiment at the CERN LHC"*, JINST 3 (2008) S08002, doi:10.1088/1748-0221/3/08/S08002.

[30] CMS Collaboration, *"Observation of a new boson with mass near 125 GeV in pp collisions at $\sqrt{s}$ = 7 and 8 TeV"*, JHEP 1306 (2013) 081, doi:10.1007/JHEP06(2013)081, arXiv:1303.4571.

[31] CMS Collaboration, *"CMS Luminosity - Public Results"*, https://twiki.cern.ch/twiki/bin/view/CMSPublic/LumiPublicResults.

[32] CMS Collaboration, *"CMS Detector Performance and Software: Technical Design Report"*, 2006. CERN/LHCC 2006-001, CMS TDR 8.1, https://cdsweb.cern.ch/record/922757/files/lhcc-2006-001.pdf.

[33] CMS Collaboration, *"The CMS magnet project: Technical Design Report"*,1997. CERN/LHCC 97-010, CMS TDR 1, http://cds.cern.ch/record/331056?ln=it.

[34] CMS Collaboration, *"Precise Mapping of the Magnetic Field in the CMS Barrel Yoke using Cosmic Rays"*, JINST 5 (2010) T03021, doi:10.1088/1748- 0221/5/03/T03021.

[35] CMS Collaboration, *"The CMS tracker system project: Technical Design Report"*,1998. CERN/LHCC 98-006, CMS TDR 5, http://cdsweb.cern.ch/record/368412.

[36] CMS Collaboration, *"The CMS tracker: addendum to the Technical Design Report"*,2000. CERN/LHCC 2000-016, CMS TDR 5.1, http://cdsweb.cern.ch/record/490194.

[37] CMS Collaboration, *"CMS Tracking Performance Results from early LHC Operation"*, Eur. Phys. J. C 70 (2010) 1165, doi:10.1140/epjc/s10052- 010-1491-3, arXiv:1007.1988.

[38] CMS Collaboration, *"Description and performance of track and primary-vertex reconstruction with the CMS tracker"*, JINST 9 (2014) P10009, doi:10.1088/1748-0221/9/10/P10009, arXiv:1405.6569.

[39] CMS Collaboration, *"The Electromagnetic Calorimeter Project: Technical Design Report"*, 1997. CERN/LHCC 97-33, CMS TDR 4, http://cds.cern.ch/record/349375?ln=it.

[40] CMS Collaboration, *"The hadron calorimeter project: technical design report"*, 1997. CERN/LHCC 97-031, CMS TDR 2, http://cdsweb.cern.ch/record/357153.

[41] CMS Collaboration, *"The muon project: Technical Design Report"*,1997. CERN/LHCC 97-032, CMS TDR 3, http://cdsweb.cern.ch/record/343814.

[42] CMS Collaboration, *"Performance of the CMS muon detector and muon reconstruction with proton-proton collisions at $\sqrt{s}$ = 13 TeV"*, JINST 13 (2018) P06015, doi:10.1088/1748-0221/13/06/P06015, arXiv:1804.04528.

[43] CMS Collaboration, *"Performance of the CMS Muon Detectors in 2016 collision runs"*, CERN-CMS-DP-2016-046, https://cds.cern.ch/record/2202964.

[44] CMS Collaboration, *"Performance of CMS muon reconstruction in pp collision events at $\sqrt{s}$ = 7 TeV"*, JINST 7 (2012) P10002, doi 10.1088/1748- 0221/7/10/P10002, arXiv 1206.4071.

[45] CMS Collaboration, *"CMS TriDAS project: Technical Design Report, Volume 1: The Trigger Systems"*, 2000. CERN/LHCC 2000-038, CMS TDR 6.1, http://cds.cern.ch/record/706847?ln=it.

[46] CMS Collaboration, *"CMS The TriDAS Project: Technical Design Report, Volume 2: Data Acquisition and High-Level Trigger"*, 2002. CERN/LHCC 2002-026, CMS TDR 6, http://cds.cern.ch/record/578006?ln=it.

[47] CMS Collaboration, *"CMS computing: Technical Design Report"*, 2005. CERN/LHCC 2005-023, CMS TDR 7, http://cds.cern.ch/record/838359?ln=it.

[48] CMS Collaboration, *"Particle-flow reconstruction and global event description with the CMS detector"*, JINST 12 (2017) P10003, doi:10.1088/1748- 0221/12/10/P10003, arXiv:1706.04965.

[49] CMS Collaboration, *"Missing transverse energy performance of the CMS detector"*, JINST 16 (2011) P09001, doi 10.1088/1748-0221/6/09/P09001, arXiv:1106.5048.

[50] P. Billoir and S. Qian, *"Simultaneous pattern recognition and track fitting by the Kalman filtering method"*, Nucl. Instrum. Meth. A 294 (1990) 219, doi:10.1016/0168-9002(90)91835-Y.

[51] Kalman, R. E., *"A New Approach to Linear Filtering and Prediction Problems"*, Journal of Basic Engineering, vol. 82, p. 35, 1960, doi:10.1115/1.3662552.

[52] P. Billoir, *"Progressive track recognition with a Kalman like fitting procedure"*, Comput. Phys. Commun. 57 (1989) 390, doi: 10.1016/0010-4655(89)90249-X.

[53] R. Fruhwirth, *"Application of Kalman filtering to track and vertex fitting"*, Nucl. Instrum. Meth. A 262 (1987) 444, doi:10.1016/0168-9002(87)90887-4.

[54] CMS Collaboration, "Measurement of the inclusive W and Z production cross sections in pp collisions at $\sqrt{s}$= 7 TeV", JHEP 10 (2011) 132, doi:10.1007/JHEP10(2011)132, arXiv:1107.4789.

[55] CMS Collaboration, CMS Tracking POG Performance Plots for 2017 Dataset.

[56] R. Fruhwirth, W. Waltenberger and P. Vanlaer, *"Adaptive Vertex Fitting"*, J. Phys. G: Nucl. Part. Phys. 34 N343 (2007), doi.org/10.1088/0954-3899/34/12/N01.

[57] CMS Collaboration, *"Muon identification and isolation efficiencies with 2017 and 2018 data"*.

[58] S. Baffioni et al., *"Electron reconstruction in CMS"*, Eur.Phys.J., vol. C49, p. 1099, 2007, doi:10.1140/epjc/s10052-006-0175-5.

[59] CMS Collaboration, *"Performance of electron reconstruction and selection with the CMS detector in proton-proton collisions at sqrt(s) =8 TeV"*, JINST 10 (2015) no.06, P06005, arXiv:1502.02701.

[60] Khachatryan, Vardan and others, *"Electron and photon performance in CMS with the full 2016 data sample"*, CMS-DP-2017-004, CERN-CMS-DP-2017-004, `https://cds.cern.ch/record/2255497/?ln=it`.

[61] CMS Collaboration, *"CMS Electron and Photon Performance at 13 TeV"*, 2019 J. Phys.: Conf. Ser. 1162 012008, doi:10.1088/1742-6596/1162/1/012008.

[62] H. Bethe and W. Heitler, *"On the Stopping of fast particles and on the creation of positive electrons"*, Proc.Roy.Soc.Lond., vol. A146, p. 83, 1934, doi:10.1098/rspa.1934.0140.

[63] W.Adam, R.Fruhwirth, A.Strandlie, and T.Todorov, *"Reconstruction of electrons with the Gaussian-sum filter in the CMS tracker at LHC"*, J. Phys. G 31 (2005) N9, doi:10.1088/0954-3899/31/9/N01, arXiv:physics/0306087.

[64] Y. Freund and R.E. Schapire, *"A Decision-Theoretic Generalization of On-Line Learning and an Application to Boosting"*, J. of Computer and System Science 55, 119 (1997), doi:10.1006/jcss.1997.1504.

[65] Sirunyan, Albert M and others, *"Identification of heavy-flavour jets with the CMS detector in pp collisions at 13 TeV "*, JINST, 13 (2018) P05011, doi: 10.1088/1748-0221/13/05/P05011, arXiv:1712.07158.

[66] M. Cacciari, G. P. Salam, and G. Soyez, *"The anti-kt jet clustering algorithm"*, JHEP, vol. 0804, 2008, doi:10.1088/1126-6708/2008/04/063, arXiv:0802.1189.

[67] X.-Y. Pham, *"Lepton flavor changing in neutrinoless tau decays"*, Eur. Phys. J. C 8 (1999) 513–516, doi:10.1007/s100529901088, arXiv:hep-ph/9810484.

[68] W. J. Marciano, T. Mori, and J. M. Roney, *"Charged Lepton Flavor Violation Experiments"*, Ann. Rev. Nucl. Part. Sci. 58 (2008) 315, doi:10.1146/annurev.nucl.58.110707.171126.

[69] S. Mihara, J. P. Miller, P. Paradisi, and G. Piredda, *"Charged Lepton Flavor-Violation Experiments"*, Ann. Rev. Nucl. Part. Sci. 63 (2013) 531–552, doi:10.1146/annurev-nucl-102912-144530.

[70] T. Sjostrand, S. Mrenna, and P. Z. Skands, *"A Brief Introduction to PYTHIA 8.1"*, Comput. Phys. Commun. 178 (2008) 852, doi:10.1016/j.cpc.2008.01.036, arXiv:0710.3820.

[71] CMS Collaboration, *"Event generator tunes obtained from underlying event and multiparton scattering measurements"*, Eur. Phys. J. C 76 (2016), no. 3, 155, doi:10.1140/epjc/s10052-016-3988-x, arXiv:1512.00815.

[72] GEANT4 Collaboration, *"GEANT4 — a simulation toolkit"*, Nucl. Instrum. Meth. A 506 (2003) 250, doi:10.1016/S0168-9002(03)01368-8.

[73] Particle Data Group Collaboration, *"Review of Particle Physics"*, Phys. Rev. D 98 (2018), no. 3, 030001, doi:10.1103/PhysRevD.98.030001.

[74] CMS Collaboration, *"Measurements of properties of the Higgs boson decaying into the four-lepton final state in pp collisions at $\sqrt{s}$ = 13 TeV"*, JHEP 11 (2017) 047, doi:10.1007/JHEP11(2017)047, arXiv:1706.09936.

[75] G. Cowan, *"Topics in statistical data analysis for high-energy physics"*, CERN Yellow Report CERN-2010-002, pp.197-218, arXiv:1012.3589.

[76] A. Hocker et al., *"TMVA - Toolkit for Multivariate Data Analysis"*, PoS ACAT (2007)040, arXiv:physics/0703039.

[77] Y. Freund and R. E. Schapire, *A short introduction to boosting*, J. Jpn. Soc. Artif. Intell. 14 (1999) 771–780, `https://cseweb.ucsd.edu/~yfreund/papers/IntroToBoosting.pdf`.

[78] T. Junk, *"Confidence level computation for combining searches with small statistics"*, Nucl. Instrum. Meth. A 434 (1999) 435, doi:10.1016/S0168-9002(99)00498-2.

[79] A. L. Read, *"Presentation of search results: the CLs technique"*, J. Phys. G: Nucl. Part. Phys. 28 (2002) 2693, doi:10.1088/0954-3899/28/10/313.